DOI: 10.1002/ejic.201000382

Application of DFT Methods in the Study of $V^{IV}O^{2+}$–Peptide Interactions

Giovanni Micera[a] and Eugenio Garribba*[a]

Keywords: Vanadium / Peptides / EPR spectroscopy / UV/Vis spectroscopy / Density functional calculations

$V^{IV}O^{2+}$ complexes formed by histidylglycylglycine (HisGlyGlyH), glycylglycylhistidine (GlyGlyHisH), glycylglycylcysteine ($GlyGlyCysH_2$), *N*-glycyl-bis(imidazol-2-yl)methylamine (Gly–BIMA), *N*-glycyl-bis(pyridin-2-yl)methylamine (Gly–BPMA), salicylglycyl-L-alanine ($SalGly\text{-}L\text{-}AlaH_2$) and 1,2-bis(2-hydroxybenzamido)benzene (H_2hybeb) in their fully deprotonated form were studied by density functional theory (DFT) methods. They are characterised by different total electric charges, total equatorial charges and number of $V–N^-_{amide}$ bonds. DFT calculations enable structural features, like V–donor bond lengths, and spectroscopic features, like electron paramagnetic resonance (EPR) and electronic absorption parameters, to be calculated. The results suggest that an amide group coordinates vanadium in the "amide-" rather than the "imine-like" form with the nitrogen atom negatively charged and with a double bond between the carbon and oxygen atoms of the carbonyl group, and that the equatorial charge is delocalised among all the donors bound to vanadium (O_{oxido} included). The analysis of the molecular orbital composition reveals that the d_{xy} orbital is the vanadium orbital at lower energy, that it can participate in a π bond with the nitrogen p_z orbital of the amide groups, that the vanadium d_{xz} and d_{yz} orbitals are involved in a large π interaction with the oxido p_x and p_y orbitals and that differences in the donor strengths of the ligands and deviations from the ideal square-pyramidal symmetry can result in the separation of the energies of the vanadium d_{xz} and d_{yz} orbitals.

Introduction

Vanadium plays a number of roles in biological systems.[1] It is found in tunicates,[2] in *Pseudopotamilla occelata*,[3] in some species of the mushroom genus *Amanita*[4] and in two enzymes, vanadium-dependent haloperoxidases (VHPOs)[5] and vanadium nitrogenase.[6] It is commonly accepted that vanadium also has an essential role in human organisms, even if its biochemical functions still remain unclear;[7] however, since it inhibits many phosphate-metabolising enzymes, such as phosphatases, ribonuclease and ATPases,[8] it has been suggested that it is involved in the regulation of phosphate metabolism. Moreover, most of its compounds show insulin-enhancing effects,[9] and the possible use of vanadium complexes in the treatment of type II diabetes is imminent.[10]

The most stable oxidation states of vanadium are +III, +IV and +V. Over the last years, it was proposed that in blood serum vanadium is mainly present in the oxidation state +IV, almost independently of the initial state,[7,11,12] and that vanadate(V) is quickly converted to the $V^{IV}O^{2+}$ ion in erythrocytes and in plasma by several reducing agents.[13]

The presence of vanadium in all of the above-mentioned systems suggests its interactions with biomolecules, and in particular with proteins and peptides.[14] Moreover, it is noteworthy that one of the most important and interesting uses of the $V^{IV}O^{2+}$ ion is as a physico-chemical marker of metal binding sites in proteins: EPR (electron paramagnetic resonance) spectroscopic patterns of the vanadyl ion have been employed since the early 1970s by Chasteen and coworkers to extract specific information on metal-binding sites of peptides and proteins such as insulin and carboxypeptidase A.[14]

Oligopeptides are the most closely related models for proteins and they can mimic specific metal ion binding sites, e.g. GlyGlyHis for serum albumin.[15] Therefore, studies on the synthetic models of the vanadium–protein interactions can greatly contribute to the knowledge of its biological activity. Oligopeptides can interact with $V^{IV}O^{2+}$ ions through the terminal amino and carboxylate groups, intermediate peptide bonds and side-chain donors, which can play the role of "anchoring groups" and promote the deprotonation of the amide bond and its coordination in the N^- form.[16] Many examples of $V^{IV}O^{2+}$ complexes containing a $V–N^-_{amide}$ bond, both in solution and in the solid state, have been characterised over the last years in the literature.[16–28]

To correctly study these systems in the absence of single-crystal X-ray diffraction analyses, it is of fundamental importance to use tools that support the usual spectroscopic techniques (EPR, UV/Vis and IR spectroscopy) to characterise the geometry, coordination mode and electronic structure of a $V^{IV}O^{2+}$–oligopeptide species. Among such tools, density functional theory (DFT) methods play a cru-

[a] Dipartimento di Chimica and Centro Interdisciplinare per lo Sviluppo della Ricerca Biotecnologica e per lo Studio della Biodiversità della Sardegna, Università di Sassari,
Via Vienna 2, 07100 Sassari, Italy
Fax: +39-079-229559
E-mail: garribba@uniss.it

Supporting information for this article is available on the WWW under http://dx.doi.org/10.1002/ejic.201000382.

cial role because they have been demonstrated to give excellent results in the optimisation of the geometries of transition-metal complexes and in the prediction of molecular and spectroscopic properties, like EPR, NMR, UV/Vis and IR spectroscopic parameters.[29]

In this work the potential of DFT methods to characterise $V^{IV}O^{2+}$–oligopeptides will be illustrated. Three important tripeptides, histidylglycylglycine (HisGlyGlyH), glycylglycylhistidine (GlyGlyHisH) and glycylglycylcysteine (GlyGlyCysH_2), were examined and the results were compared with those observed for *N*-glycyl-bis(imidazol-2-yl)methylamine (Gly–BIMA),[27] *N*-glycyl-bis(pyridin-2-yl)methylamine (Gly–BPMA),[28] salicylglycyl-L-Alanine (SalGly-L-AlaH)[24] and 1,2-bis(2-hydroxybenzamido)benzene (H_2hybeb).[17,18] They are shown in Scheme 1. Our attention will be focused on the particularly interesting species with the amide group coordinating to the vanadium atom in the deprotonated form. As pointed out in the literature,[20] a critical parameter influencing the nature of the $V–N^-_{amide}$ bond is the total equatorial charge (TEC), defined as the sum of the electric charges of the four donors in the equatorial plane of the $V^{IV}O^{2+}$ species: it is –4 (SalGly-L-AlaH_2 and H_2hybeb), –3 (HisGlyGlyH and GlyGlyCysH_2), –2 (GlyGlyHisH), –2 (Gly–BIMA and Gly–BPMA, when a OH^- ion occupies the fourth equatorial position) and –1 (Gly–BIMA and Gly–BPMA, when a water molecule is the fourth equatorial ligand). The geometry, ^{51}V and ^{14}N hyperfine coupling constants measurable from EPR and ESEEM (electron spin echo envelope modulation) spectra, ^{14}N nuclear quadrupole coupling constant, UV/Vis spectra, electronic structure and molecular orbital composition of the species involving the coordination of the deprotonated amide groups were calculated and the values compared with the experimental ones.

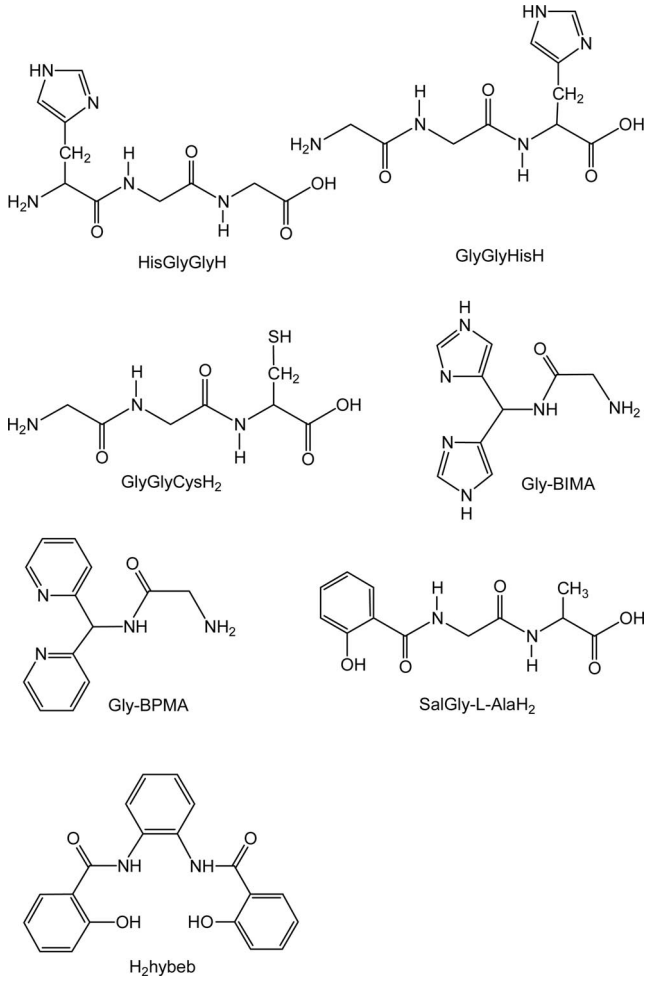

Scheme 1. Ligands studied.

Results and Discussion

Optimisation of the Structure of $V^{IV}O^{2+}$ Complexes

All the ligands were abbreviated as LH_x, with L^{x-} indicating the fully deprotonated form in aqueous solution in the absence of the metal ion. Thus, in Scheme 1 histidylglycylglycine, glycylglycylhistidine and glycylglycylcysteine are in the form LH, LH and LH_2, respectively, and can be indicated as L^-, L^- and L^{2-}, respectively, in the fully deprotonated form; the protons are lost from the –COOH group for HisGlyGlyH and GlyGlyHisH, and from –COOH and –SH for GlyGlyCysH_2.[26] Around the critical physiological pH, the two –CONH groups of HisGlyGlyH, GlyGlyHisH and GlyGlyCysH_2 undergo deprotonation to give $[VO(HisGlyGlyH_{-2})]^-$, $[VO(GlyGlyHisH_{-2})]^-$ and $[VO(GlyGlyCysH_{-2})]^{2-}$, respectively; the negative index for protons indicates the dissociation of the two amides, which do not deprotonate in the absence of $V^{IV}O^{2+}$ coordination.[26] The different electric charges are due to the presence of a LH_{-2}^{3-} ligand in the first two cases and LH_{-2}^{4-} in the third one.

The geometry of the complexes was optimised performing DFT calculations with the Gaussian 03 software.[30] The structures obtained for HisGlyGlyH, GlyGlyHisH and GlyGlyCysH_2, calculated at the level of theory B3LYP/6-311g, are represented in Figure 1; the structures of all the other complexes are shown in Figures S1–S6 of the Supporting Information.

It is known from the literature that the use of DFT methods gives rather good results in the optimisation of the geometries of transition-metal complexes, even when the calculation was performed in the gas phase.[31,32] In this work, the functional B3LYP was chosen:[33,34] its suitability to predict structures and energetics of several metal compounds, among which is vanadium,[35] is well documented. We recently evidenced that the basis set 6-311g provides results that are in good agreement with the experimental bond lengths and angles of 24 representative $V^{IV}O^{2+}$ complexes, with a reasonable calculation time.[36] It is noteworthy that when the ligand contains S atoms the use of diffuse and polarization functions [6-311+g(d) or 6-311+g*] on the sulfur is necessary to obtain values of the bond lengths that are in agreement with the experimental ones;[36] this also allows for improving the prediction of the EPR spectroscopic parameters.

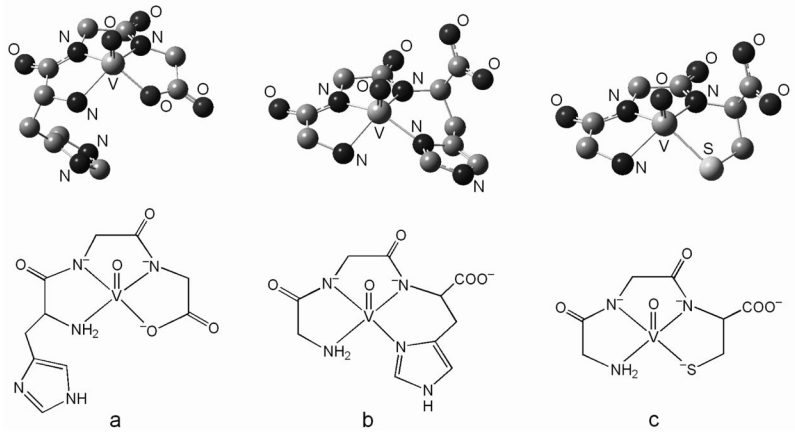

Figure 1. Optimised and molecular structures of the complexes (a) $[VO(HisGlyGlyH_{-2})]^-$, (b) $[VO(GlyGlyHisH_{-2})]^-$ and (c) $[VO(GlyGlyCysH_{-2})]^{2-}$ (see Table 1). The hydrogen atoms have been omitted for clarity.

Table 1. Details and structural parameters of the DFT calculations on $V^{IV}O^{2+}$ complexes and comparison with similar species reported in the literature.[a]

Complex[b]	V=O	V–NH_2	V–N^-_{amide}	V–O[c]	V–N_{imid}	V–N_{pyr}	V–S^-
$[VO(HisGlyGlyH_{-2})]^-$	1.615	2.153	2.002, 1.985	1.979	4.823	–	–
$[VO(GlyGlyHisH_{-2})]^-$	1.611	2.190	1.974, 1.988	3.873, 4.405	2.135	–	
$[VO(GlyGlyCysH_{-2})]^{2-}$	1.620	2.176	2.003, 1.990	3.908, 4.023	–	–	2.399
$[VO(Gly–BIMAH_{-1})(H_2O)]^+$	1.586	2.152	1.989	2.089	2.050, 5.191[d]	–	–
$[VO(Gly–BIMAH_{-1})(OH)]$	1.607	2.149	2.063	1.857	2.087, 5.248[d]	–	–
$[VO(Gly–BPMAH_{-1})(H_2O)]^+$	1.592	2.164	1.936	2.094		2.092, 5.273	–
$[VO(Gly–BPMAH_{-1})(OH)]$	1.613	2.160	1.989	1.864	–	2.128, 5.248	–
$[VO(SalGly\text{-}L\text{-}AlaH_{-2})]^{2-}$	1.620	–	2.040, 2.008	1.963, 2.032	–	–	–
$[VO(hybebH_{-2})]^{2-}$	1.613	–	2.075, 2.076	1.959, 1.959	–	–	–
$[VO(hybebH_{-2})]^{2-}$[e]	1.580	–	2.008, 1.976	1.784, 1.829	–	–	–
$[VO(hypybH_{-2})]^-$[e]	1.585	–	2.016, 2.001	1.888	–	2.108	–
$[VO(bpbH_{-2})(H_2O)]$[f]	1.607	–	2.015, 2.014	–	–	2.151, 2.149	–
$[VO(mpgH_{-1})(phen)]^-$[g]	1.602	–	2.014	1.997	–	2.173, 2.343[h]	2.382
$[VO(capcahH_{-1})(imid)]^+$[i]	1.592	–	2.012	–	2.104	2.093, 2.360[h]	–
$[VO(Gly\text{-}L\text{-}ValH_{-1})(phen)]$[j]	1.585	2.158	1.979	1.976	–	2.154, 2.348[h]	–
$[VO(MeCys)_2]$[k]	1.616	2.132	–	–	–	–	2.322

[a] All the distances are in Å. [b] Hhypyb, 1-(2-hydroxybenzamido)-2-(2-pyridinecarboxamido)benzene; bpb, 1,2-bis(2-carboxamido-pyridyl)benzene; $mpgH_2$, *N*-(2-mercaptopropionyl)glycine; phen, 1,10-phenanthroline; capcah, *N*-{2-[(pyridylmethyl)amino]phenyl}pyridine-2-carboxamide; imide, imidazole; Gly-L-ValH, glycyl-L-valine; MeCysH, L-methylcysteine. [c] O belonging to a COO^-, O^-_{ar}, OH^- or H_2O donor. [d] Mean values. [e] Experimental structure reported in ref.[18] [f] Experimental structure reported in ref.[21] [g] Experimental structure reported in ref.[19,20] [h] One N_{pyr} in the axial position. [i] Experimental structure reported in ref.[22] [j] Experimental structure reported in ref.[23] [k] Experimental structure reported in ref.[37]

The results of the simulations are summarised in Table 1, where a comparison with similar structures for which X-ray diffraction analyses are reported in the literature is also shown.[18–23,37]

The calculated V=O and V–NH_2 distances are in the ranges 1.586–1.620 and 2.149–2.190 Å, respectively, versus 1.580–1.616 and 2.132–2.158 Å, respectively, for the experimental results. The lengths of the V–N^-_{amide} bonds are in reasonable agreement with those reported for similar cases: they are between 1.974 and 2.003 Å for $[VO(HisGlyGlyH_{-2})]^-$, $[VO(GlyGlyHisH_{-2})]^-$ and $[VO(GlyGlyCysH_{-2})]^{2-}$ and between 1.976 and 2.106 Å for $[VO(hybebH_{-2})]^{2-}$,[18] $[VO(hypybH_{-2})]^-$,[18] $[VO(mpgH_{-1})(phen)]^-$,[19,20] $[VO(bpbH_{-2})(H_2O)]$,[21] $[VO(capcahH_{-1})(imid)]$[22] and $[VO(Gly\text{-}L\text{-}ValH_{-1})(phen)]$,[23] all with one or two V–N^-_{amide} bonds. The V–N^-_{amide} distances calculated for $[VO(Gly–BIMAH_{-1})(H_2O)]^+$ and $[VO(Gly–BPMAH_{-1})(H_2O)]^+$ are significantly shorter (1.989 and 1.936 Å, respectively) for the presence of the long V–OH_2 bond in the *trans* position (see Figures S1–S4). The bonds V–COO^- (1.979 Å), V–N_{imid} (2.135 Å) and V–S^- (2.399 Å) calculated for $[VO(HisGlyGlyH_{-2})]^-$, $[VO(GlyGlyHisH_{-2})]^-$ and $[VO(GlyGlyCysH_{-2})]^{2-}$, respectively, are comparable with the analogous experimentally determined bond lengths of $[VO(Gly\text{-}L\text{-}ValH_{-1})(phen)]$ (1.976 Å),[23] $[VO(capcahH_{-1})(imid)]$ (2.104 Å)[22] and $[VO(mpgH_{-1})(phen)]^-$ (2.382 Å).[20,21]

Interestingly, DFT methods give valuable information on the possible interaction of side-chain groups with vanadium. For example, they rule out the possible axial interaction of the imidazole nitrogen of the histidine residue in the *N*-terminal position for $[VO(HisGlyGlyH_{-2})]^-$ and the terminal carboxylate group for $[VO(GlyGlyHisH_{-2})]^-$ and $[VO(GlyGlyCysH_{-2})]^{2-}$, which in principle could lead to the closure of an additional chelate ring (Figure 1). In the

optimised structures the distance V–N_{imid} is 4.823 Å and those for V–COO^- are in the range 3.873–4.405 Å (Table 1). Similarly, for $[VO(Gly–BIMAH_{-1})(H_2O)]^+$, $[VO(Gly–BIMAH_{-1})(OH)]$, $[VO(Gly–BPMAH_{-1})(H_2O)]^+$ and $[VO(Gly–BPMAH_{-1})(OH)]$ the distance between vanadium and the second aromatic ring (imidazole for Gly–BIMA and pyridine for Gly–BPMA) is more than 5 Å (Table 1).

Calculation of ^{51}V and ^{14}N Hyperfine Coupling Constants

It is already known that ^{51}V hyperfine coupling constants can be measured from an EPR spectrum.[38–41] In particular, the hyperfine coupling constant along the z axis (A_z) allows for the identification of the equatorial donors of a $V^{IV}O^{2+}$ species through the application of the "additivity rule".[38,41] Unfortunately, the short relaxation times in EPR spectroscopy produce lines that are considerably broad (typically linewidths are around 10 Gauss) and this precludes, in most cases, resolution of the coupling of the unpaired electron on vanadium with the nuclei in the ligand sphere, quantified by the superhyperfine coupling constant A^L (where L indicates a generic ligand). The superhyperfine coupling constants for ^{14}N are around 4–8 MHz and vary with the nature and orientation of the ligands. ESEEM is a variant of EPR spectroscopy that can provide this superhyperfine coupling information.[41–44]

Many articles have recently been published on the possibility of predicting the ^{51}V hyperfine coupling constants in the EPR spectra of $V^{IV}O^{2+}$ species.[29,35b,45–49] The hyperfine coupling tensor A consists of three parts, the Fermi contact (A_{iso}), the anisotropic or dipolar hyperfine tensor (T) and the second-order spin-orbit tensor (A^{SO}) [see Equations (1), (2) and (3)].[48]

$$A_x = A_{iso} + T_x + A_x^{SO} \quad (1)$$

$$A_y = A_{iso} + T_y + A_y^{SO} \quad (2)$$

$$A_z = A_{iso} + T_z + A_z^{SO} \quad (3)$$

A DFT method for calculating the A tensor has been incorporated into the Gaussian 03 program,[30] which however does not include relativistic effects or spin-orbit contributions ($A_{x,y,z}^{SO}$ terms). Saladino and Larsen have shown that the best overall agreement with experimental A values can be obtained from the non-relativistic method and the half-and-half hybrid functionals:[47a] the A_{iso} values calculated deviate by about 10% from the experimental ones, whereas those calculated from the relativistic effects and pure generalised gradient correction functionals, such as BP86, deviate systematically by approximately 40%. The two authors ascribed to the possibility of the half-and-half hybrid functionals for treating core shell spin polarization the difference in performance of the two methods.[47a] We recently reached consistent progress in the prediction of the ^{51}V hyperfine coupling constants A_z, calculating A_z at the level of theory BHandHLYP/6-311g(d,p) for 22 representative $V^{IV}O^{2+}$ complexes with different charges, geometries and coordination modes with a mean deviation of 2.7% from the reported values.[49] The theoretical reasons for the agreement between the experimental and calculated A_z values depend on two facts: (i) the effect of the spin-orbit coupling (A_z^{SO}), always negative for a d^1 configuration, can be considered negligible so that A_z is described well by only two terms, A_{iso} and T_z or, alternatively, (ii) A_{iso} may be slightly overestimated and T_z slightly underestimated (or vice versa) so that the accidental compensation of such terms can result in a correct prediction of A_z (providing, however, a great help in the attribution of the experimental spectra). These two possibilities are currently under investigation in our research group. The results of the simulations are presented in Table 2.

It is observed that for all the cases the percentage deviation of the calculated A_z value is lower than 3.0% from the experimental results, supporting an [NH_2, N^-_{amide}, N^-_{amide}, COO^-] coordination for $[VO(HisGlyGlyH_{-2})]^-$, [NH_2, N^-_{amide}, N^-_{amide}, N_{imid}] coordination for $[VO(GlyGlyHisH_{-2})]^-$, [NH_2, N^-_{amide}, N^-_{amide}, S^-] coordination for $[VO(GlyGlyCysH_{-2})]^{2-}$, [($NH_2$, N^-_{amide}, N_{imid}); H_2O] and [(NH_2, N^-_{amide}, N_{imid}); OH^-] coordination for $[VO(Gly–BIMAH_{-1})(H_2O)]^+$ and $[VO(Gly–BIMAH_{-1})(OH)]$, respectively, [(NH_2, N^-_{amide}, N_{pyr}); H_2O] and [(NH_2, N^-_{amide}, N_{pyr}); OH^-] coordination for $[VO(Gly–BPMAH_{-1})(H_2O)]^+$ and $[VO(Gly–BPMAH_{-1})(OH)]$, [O^-_{ar}, N^-_{amide}, N^-_{amide},

Table 2. ^{51}V hyperfine coupling constants for $V^{IV}O^{2+}$ complexes calculated at the level BHandHLYP/6-311g(d,p).[a]

Complex	A_{iso}^{calcd}	T_x^{calcd}	T_y^{calcd}	T_z^{calcd}	A_x^{calcd}	A_y^{calcd}	A_z^{calcd}	A_z^{exptl}	$\%\|A_z\|$[b]
$[VO(HisGlyGlyH_{-2})]^-$	–88.9	32.3	36.5	–68.8	–56.6	–52.4	–157.7	–158.6[c]	–0.6
$[VO(GlyGlyHisH_{-2})]^-$	–87.9	32.7	34.9	–67.6	–55.2	–53.0	–155.5	–152.9[c]	+1.7
$[VO(GlyGlyCysH_{-2})]^{2-}$	–84.6	33.4	34.3	–67.7	–51.2	–50.3	–152.3	–147.9[c]	+3.0
$[VO(GlyGlyCysH_{-2})]^{2-}$[d]	–79.3	33.5	34.8	–68.3	–45.8	–44.5	–147.6	–147.9[c]	–0.2
$[VO(Gly–BIMAH_{-1})(H_2O)]^+$	–99.7	33.3	34.9	–68.2	–66.4	–64.8	–167.9	–163/–165[e,f]	+1.8/–3.0
$[VO(Gly–BIMAH_{-1})(OH)]$	–93.1	32.8	35.7	–68.5	–60.3	–57.4	–161.6	–160.0[e]	+1.0
$[VO(Gly–BPMAH_{-1})(H_2O)]^+$	–99.0	32.3	35.5	–67.8	–66.7	–63.5	–166.8	–162.5[g]	+2.6
$[VO(Gly–BPMAH_{-1})(OH)]$	–92.8	31.7	36.2	–67.9	–61.1	–56.6	–160.7	–158.8[g]	+1.2
$[VO(SalGly\text{-}L\text{-}AlaH_{-2})]^{2-}$	–86.1	32.3	37.2	–69.5	–53.8	–48.9	–155.6	–159[h]	–2.1
$[VO(hybebH_{-2})]^{2-}$	–90.8	30.7	37.9	–68.6	–60.1	–52.9	–159.4	–156.2[i]	+2.0

[a] All the values are given in 10^{-4} cm^{-1}. [b] Mean of the absolute percentage deviation from the experimental value: $100 \times [(|A_z|^{calcd.} - |A_z|^{exptl})/|A_z|^{exptl}]$. [c] Data reported in ref.[26] [d] Parameters calculated at the level of theory BHandHLYP/6-311+g. [e] Data reported in ref.[27] [f] Parameters that can not be measured exactly for the presence of more than one species in aqueous solution. [g] Data reported in ref.[28] [h] Data reported in ref.[24] [i] Data reported in ref.[18]

COO^-] coordination for $[VO(SalGly\text{-}L\text{-}AlaH_{-2})]^{2-}$ and finally an [O^-_{ar}, N^-_{amide}, N^-_{amide}, O^-_{ar}] coordination for $[VO(hybebH_{-2})]^{2-}$.

Therefore, DFT methods can be helpful to evaluate the coordination mode when two or more possibilities may be realised; for example, for $[VO(GlyGlyHisH_{-2})]^-$ and $[VO(GlyGlyCysH_{-2})]^{2-}$, they allow for distinguishing [NH_2, N^-_{amide}, N^-_{amide}, N_{imid}] and [NH_2, N^-_{amide}, N^-_{amide}, S^-] coordinations from the equally possible [NH_2, N^-_{amide}, N^-_{amide}, COO^-]: $|A_z|^{calcd.}$ decreases from 157.7×10^{-4} cm^{-1} for [NH_2, N^-_{amide}, N^-_{amide}, COO^-], to 155.5×10^{-4} cm^{-1} for [NH_2, N^-_{amide}, N^-_{amide}, N_{imid}] and 152.3×10^{-4} cm^{-1} for the [NH_2, N^-_{amide}, N^-_{amide}, S^-] donor set. From the examination of Table 2, it emerges that, whereas the functional BHandHLYP coupled with the basis set 6-311g(d,p) gives satisfactory results for ligands with nitrogen and oxygen donors, the 6-311+g set must be used in the calculation of A_z when V–S bonds are present. Thus, $|A_z|^{calcd.}$ for $[VO(GlyGlyCysH_{-2})]^{2-}$ is 152.3×10^{-4} cm^{-1} when 6-311g(d,p) is employed and 147.6×10^{-4} cm^{-1} with 6-311+g, values that are to be compared with the experimentally found 147.9×10^{-4} cm^{-1}.[26]

Differing from the studies concerning the prediction of ^{51}V hyperfine coupling constants, to date few computational papers have been published on the calculation of the ligand superhyperfine coupling constants for transition-metal complexes[50–53] and, to the best of our knowledge, only one concerns the $V^{IV}O^{2+}$ species.[52] Several approaches have been used: for example, Saladino and Larsen used a scalar relativistic, spin-unrestricted, open-shell Kohm-Sham calculation for simulating A^N for seven $V^{IV}O^{2+}$ species,[52] whereas Neese showed that for Cu^{II} complexes hybrid functionals, such as B3LYP or PWP1, give better predictions than functionals based on the generalised gradient approximation like BP or BLYP.[51] In the absence of a systematic DFT study on the $V^{IV}O^{2+}$ species, we performed simulations at different levels of theory on $[VO(hybebH_{-2})]^{2-}$, for which the experimental values of A^N are known.[54] The best results were obtained with the half-and-half hybrid functional BHandH and with the basis set 6-311+g(d,p): a value of –6.56 versus –6.70 MHz (experimental) is predicted for A^N_{iso} and –7.04, –6.64, –6.01 versus –7.25, –6.80, –6.05 MHz (experimental) for A^N_x, A^N_y and A^N_z, respectively; the percentage deviation from the experimental absolute values is –0.2% for A^N_{iso} and between –0.7 and –2.9% for A^N_x, A^N_y and A^N_z. All the calculated A^N values are reported in Table 3.

The components of the A^N tensor are negative. As noticed in the literature,[55] since the d_{xy} ground state has no direct spin density on the ligands, the mechanism of the superhyperfine coupling is dominated by spin polarization effects; in particular, the nitrogen orbital is polarized by exchange interaction with the unpaired electron on the vanadium d_{xy} orbital and, since the β spin electron on the nitrogen lone-pair orbital receives more Coulomb repulsion from the unpaired α spin electron on the vanadium atom, a negative spin is expected to be induced on the lone-pair orbital.[56] From an examination of the values in Table 3, a difference among the magnitudes of A^N for the amine, deprotonated amide and aromatic nitrogens emerges: $|A^N_{iso}|$ (amide) > $|A^N_{iso}|$ (imidazole) ~ $|A^N_{iso}|$ (pyridine) > $|A^N_{iso}|$ (amine). This series confirms the experimental results.[57] The values of A^N can be correlated with the s content of the sp^n-hybrid nitrogen lone pair, which undergoes the polarization mechanism. Unlike what has previously been proposed,[54] from our data $|A^N_{iso}|$ for a deprotonated amide group is slightly larger than that of an aromatic (belonging to an imidazole or pyridine ring) nitrogen, so that it could be possible to distinguish their coordination to vanadium from the $|A^N_{iso}|$ value. It will be interesting to see whether the future experimental determinations will confirm these predictions.

Calculation of ^{14}N Nuclear Quadrupolar Coupling Constants

The ^{14}N nuclear quadrupole coupling constant (NQCC or C^N_Q) is the coupling between the nuclear quadrupole moment of the nitrogen nucleus (^{14}N, $I = 1$) and the electric field gradient (EFG) at the nucleus from a nonspherical charge distribution. Nuclear quadrupole coupling constants for nitrogen are sensitive to the electronic environment of the nitrogen nucleus and can be measured experimentally in the gas and solid phase, and in solution using microwave spectroscopy, nuclear quadrupole resonance (NQR) or ESEEM spectroscopy.[54,57,58] To the best of our knowledge, the only systematic attempt to calculate C^N_Q for $V^{IV}O^{2+}$

Table 3. ^{14}N superhyperfine coupling constants for the $V^{IV}O^{2+}$ complexes calculated at the level BHandH/6-311+g(d,p).[a]

	NH_2				N^-_{amide}				N^-_{amide}				$N_{pyr/imid}$			
Complex	A^N_{iso}	A^N_x	A^N_y	A^N_z	A^N_{iso}	A^N_x	A^N_y	A^N_z	A^N_{iso}	A^N_x	A^N_y	A^N_z	A^N_{iso}	A^N_x	A^N_y	A^N_z
$[VO(HisGlyGlyH_{-2})]^-$	–3.83	–4.16	–3.95	–3.40	–7.39	–7.25	–6.98	–7.94	–7.36	–7.19	–7.17	–7.73	–	–	–	–
$[VO(GlyGlyHisH_{-2})]^-$	–4.45	–4.65	–4.51	–4.18	–7.65	–7.40	–7.27	–8.30	–7.62	–7.50	–7.34	–8.01	–5.85	–5.83	–5.04	–6.66
$[VO(GlyGlyCysH_{-2})]^{2-}$	–4.25	–4.50	–4.32	–3.94	–7.13	–6.98	–6.69	–7.72	–7.47	–7.36	–7.33	–7.73	–	–	–	–
$[VO(Gly–BIMAH_{-1})(H_2O)]^+$	–5.13	–5.36	–5.25	–4.79	–7.17	–6.92	–6.82	–7.78	–	–	–	–	–6.95	–7.47	–7.08	–6.29
$[VO(Gly–BIMAH_{-1})(OH)]$	–1.88	–2.32	–2.07	–1.25	–5.68	–6.10	–5.71	–5.24	–	–	–	–	–4.71	–5.27	–4.96	–3.91
$[VO(Gly–BPMAH_{-1})(H_2O)]^+$	–5.23	–5.48	–5.35	–4.87	–7.65	–7.32	–7.15	–8.49	–	–	–	–	–6.56	–6.44	–6.02	–7.22
$[VO(Gly–BPMAH_{-1})(OH)]$	–1.99	–2.42	–2.18	–1.36	–6.48	–6.44	–5.93	–7.06	–	–	–	–	–4.54	–4.48	–3.61	–5.54
$[VO(SalGly\text{-}L\text{-}AlaH_{-2})]^{2-}$	–	–	–	–	–7.13	–6.51	–7.13	–7.74	–7.06	–6.98	–6.75	–7.44	–	–	–	–
$[VO(hybebH_{-2})]^{2-}$[b]	–	–	–	–	–6.56	–7.04	–6.64	–6.01	–6.56	–7.04	–6.64	–6.01	–	–	–	–

[a] All the values are given in MHz. [b] Experimental data reported in ref.[54]: $|A^N_{iso}| = 6.70$, $A^N_z = –7.25$, $A^N_y = –6.80$, $A^N_z = –6.05$ MHz.

Table 4. ^{14}N nuclear quadrupolar coupling constant (C_Q^N) and asymmetry parameter η calculated at the level B3PW91/6-311+g(d,p).[a]

	NH_2		N^-_{amide}		N^-_{amide}		$N_{pyr/imid}$	
Complex	C_Q^N	η	C_Q^N	η	C_Q^N	η	C_Q^N	η
$[VO(HisGlyGlyH_{-2})]^-$	–3.60	0.34	2.79	0.12	2.96	0.41	–	–
$[VO(GlyGlyHisH_{-2})]^-$	–3.58	0.13	2.70	0.41	2.77	0.65	–2.54	0.60
$[VO(GlyGlyCysH_{-2})]^{2-}$	–3.83	0.21	2.81	0.20	2.84	0.41	–	–
$[VO(Gly–BIMAH_{-1})(H_2O)]^+$	–3.21	0.22	3.15	0.57	–	–	–2.02	0.84
$[VO(Gly–BIMAH_{-1})(OH)]$	–3.74	0.27	3.45	0.26	–	–	–2.38	0.74
$[VO(Gly–BPMAH_{-1})(H_2O)]^+$	–3.19	0.21	2.82	0.66	–	–	–2.55	0.24
$[VO(Gly–BPMAH_{-1})(OH)]$	–3.67	0.26	3.20	0.44	–	–	–3.24	0.04
$[VO(SalGly\text{-}L\text{-}AlaH_{-2})]^{2-}$	–	–	2.91	0.29	2.89	0.26	–	–
$[VO(hybebH_{-2})]^{2-}$[b]	–	–	2.91	0.12	2.91	0.12	–	–

[a] All the values are given in MHz. [b] Experimental data reported in ref.[54]: C_Q = 2.5 MHz, η = 0.04.

complexes was performed by Saladino and Larsen, who used two different types of calculations: a scalar-relativistic, spin-unrestricted, open-shell Kohn–Sham (SR UKS) approach and another scalar-relativistic, spin-restricted, open-shell Kohn–Sham with determination of the spin-orbit coupling (SO + SR ROKS).[52] The results were invariant with respect to the computational method, with deviations between the calculated and experimental values in the range 5–25% and an average deviation of 14%. As for the ^{14}N superhyperfine coupling constant, we calculated C_Q^N at different levels of theory for $[VO(hybebH_{-2})]^{2-}$, the only compound among those studied in this work with a known value of C_Q^N (2.50 MHz).[54] The best results were obtained with the functional B3PW91 and basis set 6-311+g(d,p), from which a value of 2.91 MHz was obtained. Other combinations of functionals and basis sets afforded larger deviations. The possible use of the basis set 6-311+g(d,p) has been suggested by Crans and Polenova for V^V complexes.[59] The values of C_Q^N for the complexes studied are listed in Table 4.

DFT calculations predict a negative sign of C_Q^N for amine and imidazole or pyridine nitrogens, and a positive sign for a deprotonated amide nitrogen. With regard to the magnitude of C_Q^N, it is expected that $|C_Q^N|$ (amine) > $|C_Q^N|$ (amide) > $|C_Q^N|$ (imidazole) ≈ $|C_Q^N|$ (pyridine). This is in agreement with the fact that the absolute value of the nitrogen nuclear quadrupole coupling constant for an amine is higher than that for an imine. In this case too, the experimental measurement of C_Q^N may confirm whether our suppositions are correct.

Calculation of the UV/Vis Spectra

The electronic absorption spectra of complexes formed by peptides exhibit, besides the normal d–d transitions, intense charge-transfer bands below 400 nm; in particular, an absorption in the region 200–300 nm is characteristic of the coordination of an amide deprotonated bond.[60] To help with the assignment of the observed bands and evaluate the properties of the excited states, TD-DFT methods can be employed that, after their recent implementations, are nowadays frequently used in the simulations of the electronic transitions of metal ion complexes.[29,61,62]

TD-DFT methods calculate the vertical excitation energies from the ground state. The electronic structures of the excited states are described in terms of multiconfigurations: this means that a linear combination of excitations from occupied to virtual molecular orbitals (MO) comprises a given electronic transition. Consequently, the dominant character of each transition can be specified, but keeping in mind that this only contributes to a certain percentage. TD-DFT methods also provide the electric dipole oscillator strength (f) of the transition from the ground to the excited

Table 5. Main calculated and experimental electronic transitions for $[VO(HisGlyGlyH_{-2})]^-$.

Most important orbital excitation	Character	λ [nm]	E [eV]	f	λ [nm]/ε [M^{-1} cm^{-1}]^{exptl}
HOMO → LUMO+1	$d_{xy} \rightarrow d_{xz}$	602.1	2.06	0.0006	580/50
HOMO → LUMO+2	$d_{xy} \rightarrow \sigma^*_{imid}$	506.9	2.45	0.0003	
HOMO → LUMO+7	$d_{xy} \rightarrow d_{x^2-y^2}$	419.0	2.96	0.0002	
HOMO → LUMO+3	$d_{xy} \rightarrow d_{yz}$	396.3	3.13	0.0004	
HOMO–1 → LUMO+1	$\pi_{amide} \rightarrow d_{xz}$	308.6	4.02	0.0040	330/1200
HOMO–2 → LUMO+1	$O^{lp}_{amide} \rightarrow d_{xz}$	280.4	4.42	0.0021	
HOMO–1 → LUMO+2	$\pi_{amide} \rightarrow \sigma^*_{imid}$	275.8	4.50	0.0044	
HOMO–1 → LUMO+2	$\pi_{amide} \rightarrow \sigma^*_{imid}$	270.7	4.55	0.0122	267/3300
HOMO–2 → LUMO+1	$\pi_{amide} \rightarrow d_{xz}$	263.8	4.70	0.0012	
HOMO–1 → LUMO+3	$\pi_{amide} \rightarrow d_{yz}$	259.1	4.78	0.0014	
HOMO–2 → LUMO+2	$O^{lp}_{amide} \rightarrow \sigma^*_{imid}$	253.6	4.89	0.0111	
HOMO–2 → LUMO	$O^{lp}_{amide} \rightarrow \pi^*_{imid}$	252.8	4.90	0.0111	
HOMO–2 → LUMO	$O^{lp}_{amide} \rightarrow \pi^*_{imid}$	252.4	4.91	0.0099	

state, which is related to the transition moment, thereby allowing the description of the electronic spectrum of a metal complex in the UV and visible region.[63]

The most important orbital transitions, their character, the excitation energies and wavelengths, and the oscillator strengths were calculated at the level B3LYP for $[VO(HisGlyGlyH_{-2})]^-$, $[VO(GlyGlyHisH_{-2})]^-$, $[VO(GlyGlyCysH_{-2})]^{2-}$, $[VO(Gly–BPMAH_{-1})(OH)]$ and $[VO(Gly–BPMAH_{-1})(H_2O)]^+$. The data for $[VO(HisGlyGlyH_{-2})]^-$ are reported in Table 5, and for the other complexes in Tables S1–S4 in the Supporting Information.

According to the TD-DFT calculations, the high mixing of excited configurations due to the low symmetry of the complexes does not allow for classifying the calculated transitions into the well-known intraligand or interligand (LL), ligand-to-metal (LMCT), metal-to-ligand (MLCT) and ligand field d–d (LF) transitions. The absorption bands arise from electronic transitions between highly delocalised molecular orbitals resulting from the mixing of excited configurations having large coefficients in the CI wave functions.

The computed electronic transitions are not always in good agreement with the experimental ones and the description that emerges is more qualitative than quantitative. The calculated and the experimental spectra for $[VO(HisGlyGlyH_{-2})]^-$ are displayed in Figure 2.

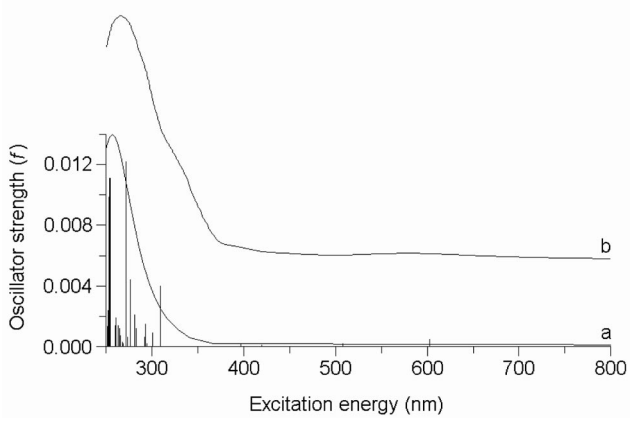

Figure 2. Calculated (a) and experimental (b) electronic absorption spectrum of $[VO(HisGlyGlyH_{-2})]^-$.

From the comparison between the two spectra (Table 5 and Tables S1–S4 in the Supporting Information), it emerges that the region between 750 and 400 nm is dominated by the electronic transitions with a significant d–d component. In particular, for $[VO(HisGlyGlyH_{-2})]^-$ the three transitions $d_{xy} \rightarrow d_{z^2}$, $d_{xy} \rightarrow d_{xz}$ and $d_{xy} \rightarrow d_{x^2-y^2}$, expected on the basis of crystal field considerations,[64] with values of the oscillator strength (related to the molar absorption coefficient ε[63]) below 0.0010, are predicted. However, these bands are composite and the possibility of a mixture between the ground and excited states must be taken into account: for example, the band calculated at 602.1 nm for $[VO(HisGlyGlyH_{-2})]^-$ has a 49.1% contribution from the $d_{xy} \rightarrow d_{xz}$ (HOMO → LUMO+1) excitation, a 32.4% contribution from the $\pi_{amide} \rightarrow d_{xz}$ (HOMO–1 → LUMO+1) excitation and a 10.9% contribution from the $d_{xy} \rightarrow \sigma^*_{imid}$ (HOMO → LUMO+2) excitation.

For wavelengths lower than 350–400 nm, depending on the particular complex, the dominant character of the electronic transitions is LMCT and MLCT and the oscillator strength associated with the transition increases. For example, the excitations $\pi_{amide} \rightarrow d_{xz}$ (HOMO–1 → LUMO+1) at 308.6 nm and $d_{xy} \rightarrow \pi^*_{imid}$ (HOMO → LUMO) at 291.0 nm can be considered to belong to such a class. However, it must be noted that these types of electronic excitations can also be observed in the visible region of the spectrum, as happens for $[VO(GlyGlyCysH_{-2})]^{2-}$, for which the $S^{lp} \rightarrow d$ character is dominant for the transitions between 650 and 300 nm (Table S2).

Finally, below 270 nm the LLCT transitions become the most important and these correspond to the highest values of the oscillator strength *f*. For example, for $[VO(HisGlyGlyH_{-2})]^-$ the most intense transition ($f = 0.0122$) is from a $\pi_{amide} \rightarrow \sigma^*_{imid}$ excitation, for $[VO(GlyGlyHisH_{-2})]^-$ ($f = 0.0171$) it is from a composite $\pi_{amide} \rightarrow \pi^*_{imid}$ plus a $O^{lp}{}_{amide} \rightarrow \pi^*_{imid}$ excitation and for $[VO(Gly–BPMAH_{-1})(H_2O)]^+$ and $[VO(Gly–BPMAH_{-1})(OH)]$ ($f = 0.0150$ and 0.0255, respectively) it is from a $\pi_{amide} \rightarrow \pi^*_{pyr}$ excitation. It is noteworthy that these transitions involve inter- rather than intraligand excitations; however, such excitations have been reported for other metal-transition complexes.[65]

Characterisation of the $V–N^-_{amide}$ Bond and its Effect on the ^{51}V A_z Value

The value of the ^{51}V hyperfine coupling constant along the *z* axis, A_z, for the $V^{IV}O^{2+}$ species can be estimated from the "additivity rule", an empirical relationship, proposed by Wüthrich[66] and developed by Chasteen[38] and Pecoraro,[41] based on the contribution to A_z from each of the four equatorial donors [Equation (4)].

$$A_z = \sum_{i=1}^{4} A_z(\text{donor } i) = A_z(\text{donor 1}) + A_z(\text{donor 2}) + A_z(\text{donor 3}) + A_z(\text{donor 4}) \quad (4)$$

The value of the contribution to A_z for the more common donor functions, like H_2O, OH^-, O^-_{ar}, RO^-, COO^-, CO, NH_2, N_{pyr}, N_{imid}, N_{imine}, S^-_{ar}, RS^-, Cl^- and SCN^-, is now reported in the literature.[22,25,38,41,67–69] With regard to the contribution of an amide group, A_z (amide), the value seems to be sensitive to the total equatorial charge and, particularly, decreases when decreasing the donation of electron density from the ligands to the metal ion.[17,20] Tasiopoulos et al. attributed the mean values of 32.2, 36.5 and 40.3×10^{-4} cm^{-1} to A_z (amide) when the total charge of the donor atoms in the equatorial plane is –2, –3 and –4, respectively (including the –1 charge of the deprotonated amide nitrogen).[20] Subsequently, we extended the analysis to 37 $V^{IV}O^{2+}$ complexes, 9 with a –4, 9 with a –3 and 19 with a –2 total charge, and slightly corrected the contribution of a deprotonated amide group to the value of A_z to

40.9 (–4), 38.3 (–3) and 35.5×10^{-4} cm^{-1} (–2); the value for the equatorial charge –1 was calculated by extra polation and resulted in a value of 32.7×10^{-4} cm^{-1}.[25]

The wide range of the A_z (amide) contribution was explained by assuming two limit resonance structures for an amide group coordinated through the nitrogen atom, one "amide-like", with the nitrogen atom negatively charged and a double bond between the carbon and oxygen atoms of the carbonyl group (Scheme 2, a), and another "imine-like" with the carbonyl oxygen negatively charged and a double bond between the carbon and nitrogen atoms (Scheme 2, b).[17,20] The predominance of one of these structures should depend on the electronic density of the metal ion and, particularly, the importance of the "amide-like" form should increase with decreasing the electronic density on the equatorial plane.

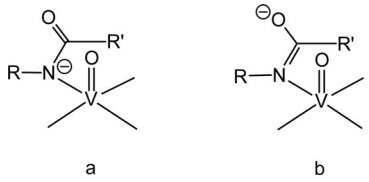

Scheme 2. Limit resonance structures for a deprotonated amide group bound to a $V^{IV}O^{2+}$ species: (a) "amide-like" and (b) "imine-like" form.

In Figure 3 the calculated V–N, C–N and C=O distances are represented as a function of the absolute value of the equatorial charge for the complexes studied (1, 2, 3 and 4). An examination reveals that they do not change significantly and always remain close to the values expected for the "amide" form. However, as the total equatorial charge decreases and the "amide-like" form becomes prevalent, the V–N and C=O bonds shorten, whilst the C–N bond slightly lengthens, suggesting that the electronic density in the equatorial plane affects the form of the amide group; for example, the V–N bond length is 1.936 for $[VO(Gly–BIMAH_{-1})(H_2O)]^+$ when the equatorial charge is –1, 1.974 and 1.988 Å for $[VO(GlyGlyHisH_{-2})]^-$ when the charge is –2, 1.990 and 2.003 Å for $[VO(GlyGlyCysH_{-2})]^{2-}$ when the charge is –3, and finally 2.008 and 2.040 Å for $[VO(SalGly\text{-}L\text{-}AlaH_{-2})]^{2-}$ when the charge is –4. For comparison, for $[VOCl(capcaH_{-1})]$ (capca is N{2-[(2-pyridylmethylene)-amino]phenyl}pyridine-2-carboxamide), which possesses both a $V–N^-_{amide}$ and a $V–N_{imine}$ bond, the predicted distances are 2.027 and 2.106 Å, respectively, versus the experimental distances of 2.010 and 2.079 Å, respectively.[22]

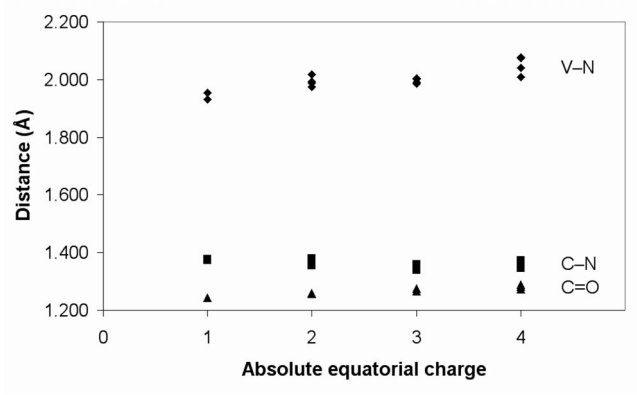

Figure 3. Lengths of V–N (rhombi), C–N (squares) and C=O (triangles) bonds as a function of the absolute value of the equatorial charge.

An analysis of Table 6 reveals that the atomic charges on the amide nitrogen atoms are comparable when the total equatorial charge changes from –1 to –4. In particular, it is very close to –1, almost independent of the charge on the equatorial plane, and ranges from –0.72 to –0.84, confirming the "amide-like" form of the group. Moreover, the C=O group is in its neutral form.

As recently observed, the only certain datum is that the decrease in the total equatorial charge of a $V^{IV}O^{2+}$ complex containing one or more $V–N^-_{amide}$ bonds always results in a decrease in the A_z value, whilst if the equatorial charge remains fixed no significant changes in the A_z value can be detected.[27] For example, by going from $[VO(hypybH_{-2})]^-$ [(N_{pyr}, N^-_{amide}, N^-_{amide}, O_{ar}^-) donor set and total equatorial charge –3, with Hhypyb 1-(2-hydroxybenzamido)-2-(2-pyridinecarboxamido)benzene] to $[VO(bpbH_{-2})]$ [(N_{pyr},

Table 6. Energy, total equatorial charge and atomic charges for $V^{IV}O^{2+}$ complexes.[a]

Complex	TEC[b]	O_{oxido}	NH_2	N^-_{amide}	O[c]	$N_{pyr/imid}$	S^-	$C_{carbonyl}$	$O_{carbonyl}$
$[VO(HisGlyGlyH_{-2})]^-$	–3	–0.63	–0.20	–0.72, –0.72	–0.68	–	–	0.54, 0.47	–0.51, –0.49
$[VO(GlyGlyHisH_{-2})]^-$	–2	–0.56	–0.21	–0.75, –0.74	–	–0.69	–	0.51, 0.49	–0.44, –0.45
$[VO(GlyGlyCysH_{-2})]^{2-}$	–3	–0.61	–0.19	–0.72	–0.71		–0.49	0.49, 0.47	–0.49, –0.50
$[VO(Gly–BIMAH_{-1})(H_2O)]^+$	–1	–0.46	–0.17	–0.78	0.09	–0.77	–	0.57	–0.46
$[VO(Gly–BIMAH_{-1})(OH)]$	–2	–0.58	–0.15	–0.74	–0.54	–0.69	–	0.54	–0.53
$[VO(Gly–BPMAH_{-1})(H_2O)]^+$	–1	–0.47	–0.17	–0.81	0.09	–0.75	–	0.53	–0.37
$[VO(Gly–BPMAH_{-1})(OH)]$	–2	–0.59	–0.16	–0.77	–0.55	–0.67	–	0.50	–0.43
$[VO(SalGly\text{-}L\text{-}AlaH_{-2})]^{2-}$	–4	–0.65	–	–0.73, –0.72	–0.64, –0.71	–	–	0.45, 0.48	–0.54, –0.54
$[VO(hybebH_{-2})]^{2-}$	–4	–0.63	–	–0.84, –0.84	–0.69, –0.69	–	–	0.46, 0.46	–0.53, –0.53

[a] Atomic charges with hydrogens summed into heavy atoms. [b] Total equatorial charge. [c] O belonging to a COO^-, O^-_{an}, OH^- or H_2O donor.

N^-_{amide}, N^-_{amide}, N_{pyr}) donor set and total equatorial charge –2, with bpb 1,2-bis(2-carboxamidopyridyl)benzene] the A_z value changes from 156.1 to 145×10^{-4} cm^{-1} even if the contribution of a pyridine nitrogen to A_z is higher (40.7×10^{-4} cm^{-1}) than a deprotonated aromatic oxygen (38.9×10^{-4} cm^{-1});[17,18,21] but, by going from [VO(thipcaH$_{-1}$)] [(N_{pyr}, N^-, N_{imino}, S_{ar}^-) donor set and total equatorial charge –2, with Hthipca *N*-{2-[(thiophenoylmethylene)-amino]phenyl}pyridine-2-carboxamide to [VO(phepcaH$_{-1}$)] [(N_{pyr}, N^-, N_{imino}, O_{ar}^-) donor set and total equatorial charge –2, with Hphepca *N*-[2-((2-Phenolylmethylene)-amino)phenyl]pyridine-2-carboxamide] the A_z value changes from 150.6 to 154×10^{-4} cm^{-1}, exactly what is predicted on the basis of the contributions to A_z of a deprotonated aromatic sulfur (35.3×10^{-4} cm^{-1}) and oxygen atoms (38.9×10^{-4} cm^{-1}).[17,18] It is obvious that in such situations if the contribution to A_z of all the other donor functions is considered constant, the decrease in A_z must be entirely attributed to the decrease in A_z (amide). However, on the basis of the results reported in Table 6, we can propose the hypothesis that all the donors should participate in the reduction of A_z, with the logical consequence that the contribution to A_z of all the equatorial donors decreases with decreasing the total equatorial charge and that the electronic density is distributed on all the donor functions bound to vanadium. Rather interestingly, with increasing the equatorial charge on the equatorial plane of the $V^{IV}O^{2+}$ ion the amount of negative charge delocalised on the oxido donor increases: it goes from –0.46 when it is –1, to –0.65 when it is –4. Therefore, we stress that there is no reason that only the deprotonated N^-_{amide} function may change its contribution to A_z with varying the equatorial charge: this is an oversimplification that is helpful when the experimental EPR spectra have to be analysed through the "additivity rule".

Analysis of Molecular Orbital (MO) Compositions

The ligand field of the complexes studied is square pyramidal with the oxido ligand occupying the *z* axis in the chosen coordinate system and the four equatorial ligands the *x* and *y* axes. In such a ligand field the five vanadium 3d orbitals normally split into d_{xy}, the doubly degenerate set d_{xz}, d_{yz}, and the single $d_{x^2-y^2}$ and d_{z^2} orbitals.[64]

As an example, the composition of the most important occupied and virtual molecular orbitals (MO) for [VO(HisGlyGlyH$_{-2}$)]$^-$ is given in Table 7, whilst the corresponding energy diagram is shown in Figure 4. The compositions of the highest occupied and lowest unoccupied molecular orbitals for the other compounds studied are listed in Tables S5–S12 of the Supporting Information.

In all the cases, the vanadium d based MO d_{xy} is at a lower energy than the other four orbitals: usually, but not always, it is the HOMO (or SOMO, singly occupied molecular orbital). It carries a certain amount of vanadium character in the range 35.0–78.1% depending on the distortion from the square-pyramidal structure and on the interaction of the vanadium d_{xy} based MO with the donor orbitals: this is illustrated in Figure 5 for [VO(GlyGlyHisH$_{-2}$)]$^-$ and [VO(GlyGlyCysH$_{-2}$)]$^-$, for which the interaction is with the nitrogen p_z based orbital of one of the two deprotonated amide groups. Analogous observations were reported for the $Mo^{V}O^{3+}$ complex with the tetradentate N_2S_2 ligand.[70]

The vanadium d_{xz} and d_{yz} orbitals interact through π bonding with the oxido p_x and p_y orbitals and they are 4.5–5.8 eV higher in energy than the vanadium d_{xy} based MO {about 5 eV for [VO(HisGlyGlyH$_{-2}$)]$^-$, Figure 4}. Such bonding shows a relevant degree of covalency, as evidenced from the oxido character mixed into the vanadium d_{xz} and d_{yz} based MOs, which is 20.9% for [VO(Gly–BPMAH$_{-1}$)(OH)] {10 and 13% for [VO(HisGlyGlyH$_{-2}$)]$^-$, Table 7}. Differences in the covalency and donor strengths of the five ligands as well as deviations from the perfect square-pyramidal symmetry decrease the effective site symmetry, which can result in the separation of the energies of the vanadium d_{xz} and d_{yz} orbitals. This orbital splitting is variable and ranges between 0.03 eV for [VO(Gly–BIMAH$_{-1}$)(H_2O)]$^+$ and 0.87 eV for [VO(Gly–BPMAH$_{-1}$)(OH)]; for [VO(Gly–BIMAH$_{-1}$)(H_2O)]$^+$, [VO(HisGlyGlyH$_{-2}$)]$^-$ and [VO(SalGly-

Table 7. Composition of the highest occupied and lowest unoccupied molecular orbitals for [VO(HisGlyGlyH$_{-2}$)]$^-$.[a]

Complex		Vanadium					Amide		Carboxylate		Imidazole		
	E [eV]	Tot.	d	O_{oxido}	NH_2	Tot.	N_{amide}	O_{amide}	Tot.	O_{carb}	Tot.	N_{imid}	C_{imid}
LUMO+7	3.88	**40.2**	40.2	4.0	5.4	17.8	7.8	3.1	19.8	9.0	1.1	0.2	0.5
LUMO+6	3.62	26.0	14.7	5.2	15.9	11.1	2.6	2.8	1.3	0.6	**32.0**	6.4	24.1
LUMO+5	3.33	**40.3**	39.2	10.6	4.0	3.5	2.3	0.3	8.0	3.8	18.0	5.1	12.6
LUMO+4	3.11	**28.9**	27.7	12.7	1.2	11.3	1.7	3.3	11.8	4.4	**27.1**	6.6	20.2
LUMO+3	2.85	**39.9**	38.1	13.1	2.5	23.1	2.6	7.1	2.4	2.1	5.6	1.4	4.0
LUMO+2	2.72	6.3	6.2	1.6	1.4	1.9	0.4	0.5	0.1	0.0	**86.6**	–7.0	–3.6
LUMO+1	2.65	**44.2**	37.7	9.7	11.6	9.9	1.7	3.1	0.5	0.2	14.1	0.5	1.5
LUMO	2.33	0.5	0.4	0.1	2.3	0.3	0.0	0.0	0.0	0.0	**95.2**	28.9	64.4
HOMO	–2.28	**62.3**	62.2	0.5	1.3	17.9	8.7	8.4	12.4	11.4	0.0	0.0	0.0
HOMO–1	–2.69	20.4	20.3	3.9	0.2	**63.8**	34.0	28.8	7.4	6.6	0.2	0.0	0.1
HOMO–2	–2.99	1.0	0.9	3.5	0.2	**79.8**	20.1	56.5	3.5	3.3	0.1	0.0	0.1
HOMO–3	–3.40	2.3	2.1	8.4	0.8	**58.8**	23.9	33.4	22.8	21.7	0.6	0.0	0.5
HOMO–4	–3.51	0.6	0.5	3.5	0.1	40.0	16.2	22.9	**47.3**	45.3	0.1	0.0	0.1
HOMO–5	–3.68	5.0	5.0	0.3	1.2	**68.8**	5.8	59.8	13.2	12.4	0.7	0.1	0.6

[a] Main contributions are shown in bold font.

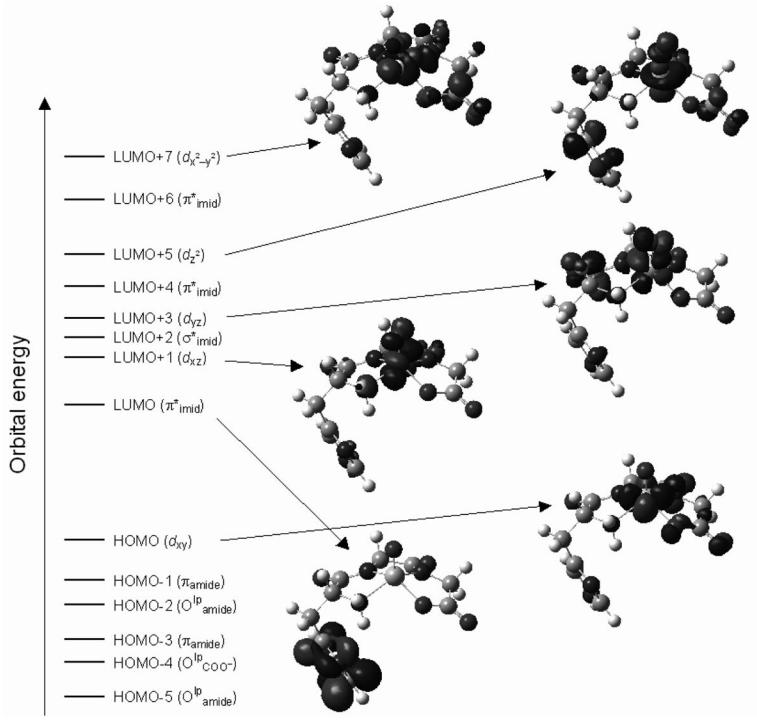

Figure 4. Molecular orbital diagram for $[VO(HisGlyGlyH_{-2})]^-$. Note that the energy levels are not to scale.

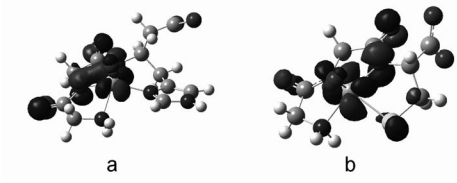

Figure 5. π-Bonding interaction between the vanadium d_{xy} and nitrogen p_z orbital in (a) $[VO(GlyGlyHisH_{-2})]^-$ and (b) $[VO(GlyGlyCysH_{-2})]^-$.

L-$AlaH_{-2})]^{2-}$ the separation is below 0.1 eV, so the two orbitals can be considered almost degenerate.

The two higher vanadium d_{z^2} and $d_{x^2-y^2}$ based MOs at higher energy are antibonding between the vanadium and oxido group on the one hand, and vanadium and the equatorial ligands on the other; the strong interaction between the vanadium $d_{x^2-y^2}$ orbital and the orbitals of the equatorial donors pushes it up in energy.

The donor strength of the different ligands is reflected in the Wiberg bond orders collected in Table 8. It is clearly seen that the oxido is by far the strongest donor with a calculated bond order in the range 1.829–2.016, consistent with a formal double bond between this ligand and the central vanadium atom. The calculated orders for the $V–N^-_{amide}$ bonds in $[VO(HisGlyGlyH_{-2})]^-$, $[VO(GlyGlyHisH_{-2})]^-$, $[VO(GlyGlyCysH_{-2})]^{2-}$, $[VO(SalGly\text{-}L\text{-}AlaH_{-2})]^{2-}$ and $[VO(hybebH_{-2})]^{2-}$ are not equivalent, consistent with the differences in the bond lengths observed in crystal structures and structure optimisation (Table 1), and with their significantly different orientation relative to the vanadium d_{xy} based MO. The strength of a $V–N^-_{amide}$ is comparable with that of the $V–O^-_{ar}$ bond in $[VO(SalGly\text{-}L\text{-}AlaH_{-2})]^{2-}$ and $[VO(hybebH_{-2})]^{2-}$. Among the other V-donor bonds, $V–OH^-$ and $V–S^-$ (0.570–0.584 and 0.566, respectively) are stronger than $V–NH_2$, $V–N_{imid}$ and $V–N_{pyr}$, which strongly depend on the strength of the donor atom in the *trans* posi-

Table 8. Wiberg bond indices for $V^{IV}O^{2+}$ complexes.

	V=O	V–NH_2	V–N^-	V–N[a]	V–O[b]	V–S
$[VO(HisGlyGlyH_{-2})]^-$	1.838	0.242	0.401, 0.468		0.419	
$[VO(GlyGlyHisH_{-2})]^-$	1.874	0.235	0.493, 0.503	0.239		
$[VO(GlyGlyCysH_{-2})]^{2-}$	1.836	0.226	0.419, 0.477			0.566
$[VO(Gly–BIMAH_{-1})(H_2O)]^+$	2.014	0.293	0.534	0.315	0.167	
$[VO(Gly–BIMAH_{-1})(OH)]$	1.895	0.264	0.374	0.257	0.584	
$[VO(Gly–BPMAH_{-1})(H_2O)]^+$	2.016	0.336	0.603	0.335	0.193	
$[VO(Gly–BPMAH_{-1})(OH)]$	1.879	0.266	0.404	0.253	0.570	
$[VO(SalGly\text{-}L\text{-}AlaH_{-2})]^{2-}$	1.829		0.390, 0.409		0.393, 0.357	
$[VO(hybebH_{-2})]^{2-}$	1.865		0.353, 0.354		0.400, 0.400	

[a] N belonging to an imidazole or pyridine nitrogen. [b] O belonging to a COO^-, O^-_{ar}, OH^- or H_2O donor.

tion. Finally, the neutral water molecule is by far the weakest in the ligand sphere.

Very similar results are obtained if the Mayer instead of the Wiberg bond orders are considered (Table S13 of Supporting Information).

The spin distribution for the studied complexes, as obtained from the DFT calculations (Table 9), shows that almost the whole of the spin population (1.12–1.17) is localised on the vanadium atom. However, a significant negative spin population (between –0.13 and –0.16) is predicted on the terminal oxido donor. Indeed, a negative spin density on the terminal oxygen atom has been found for $[Cr^{V}O(benzene\text{-}1,2\text{-}dithiolato)_2]^{2-}$[71] and suggested for $[Mo^{17}O(PhS)_4]^-$ on the basis of the experimentally measured hyperfine and nuclear quadrupole interaction parameters for the oxido-^{17}O ligand.[72] This negative spin density may originate from spin-polarization mechanisms.

Table 9. Spin densities for vanadium and oxido ligand in $V^{IV}O^{2+}$ complexes.

	V	O
$[VO(HisGlyGlyH_{-2})]^-$	1.135910	–0.132087
$[VO(GlyGlyHisH_{-2})]^-$	1.142375	–0.141258
$[VO(GlyGlyCysH_{-2})]^{2-}$	1.149324	–0.134390
$[VO(Gly–BIMAH_{-1})(H_2O)]^+$	1.170653	–0.162263
$[VO(Gly–BIMAH_{-1})(OH)]$	1.124354	–0.144027
$[VO(Gly–BPMAH_{-1})(H_2O)]^+$	1.169167	–0.160439
$[VO(Gly–BPMAH_{-1})(OH)]$	1.116517	–0.141824
$[VO(SalGly\text{-}L\text{-}AlaH_{-2})]^{2-}$	1.125430	–0.132475
$[VO(hybebH_{-2})]^{2-}$	1.131865	–0.140351

Conclusions

In order to understand the role of vanadium in the organism and the mechanism of action of the insulin-enhancing compounds it seems to be essential to know the interaction of vanadium with oligopeptides and proteins. Peptides are molecules provided with lots of groups, like the terminal amino and carboxylate, the intermediate peptide bonds and the side-chain donors. Therefore, in the absence of X-ray diffraction analysis on the single crystal, it is not easy to interpret the results of the spectroscopic measurements. Thus, it is desirable to have some tool able to gain insights into the characterisation of these complicated systems.

This work demonstrates that DFT calculations are a suitable method to characterise the structure and spectroscopic properties of the $V^{IV}O^{2+}$ complexes formed by oligopeptides. They can reproduce the coordination sphere around vanadium with a satisfactory degree of accuracy and can suggest whether a specific group is interacting with the metal ion: for example, for HisGlyGlyH, GlyGlyHisH and $GlyGlyCysH_2$, they rule out the axial interaction of the imidazole nitrogen of the hystidine residue in the first case and the carboxylates of histidine and cysteine in the other two.

DFT calculations can also provide helpful information in the interpretation of EPR, ESEEM and UV/Vis spectra. Whilst an electronic absorption spectrum is reproduced only qualitatively, the ^{51}V hyperfine coupling constant along the z axis (A_z) measured in the EPR spectra can be calculated with a deviation from the experimental value that is within 3%. Helpful information concerning the values of the ^{14}N superhyperfine coupling constant (A^N) and ^{14}N nuclear quadrupole coupling constant (NQCC or C_Q^N) is also obtained. Thus, the combined examination of the predicted EPR, ESEEM and electronic absorption data can be of great help in the characterisation of the coordination mode of an oligopeptide. For HisGlyGlyH, GlyGlyHisH and $GlyGlyCysH_2$, the DFT simulations enable the coordination modes from [NH_2, N^-_{amide}, N^-_{amide}, COO^-], [NH_2, N^-_{amide}, N^-_{amide}, N_{imid}] and [NH_2, N^-_{amide}, N^-_{amide}, S^-], respectively, to be distinguished.

Finally, DFT methods can be useful to describe the electronic structure of the species formed. In particular, they suggest that the charge of the complexes is delocalised among all the donors bound to vanadium and that an amide group coordinates vanadium in the "amide-" rather than "imine-like" form with the nitrogen atom negatively charged. This result must be taken into account in the application of the "additivity rule" to calculate the A_z value of an EPR spectrum. The analysis of the molecular orbital composition reveals the presence of π bonds between the vanadium d_{xy} and nitrogen p_z orbitals of the amide group, and between the vanadium d_{xz} and d_{yz} and oxido p_x and p_y orbitals.

Of course, these results can also be applied to the studies in which the $V^{IV}O^{2+}$ ion is used as a physico-chemical marker of metal-binding sites in proteins, in particular in the case of albumin.

Computational Section

DFT Calculations: All calculations presented in this paper were performed using the Gaussian 03 program (revision C.02)[30] and DFT methods.[73]

For the geometry optimisation, the hybrid exchange-correlation functional B3LYP was employed.[33,34] The geometries were firstly pre-optimised at the level B3LYP/sto-3g and further optimised at the level of theory B3LYP/6-311g. For $[VO(GlyGlyCysH_{-2})]^{2-}$ the basis set 6-311+g(d) was used on the sulfur atom. For all the structures, minima were verified through frequency calculations.

The optimised structures were used to calculate the ^{51}V hyperfine (A_{iso}, A_x, A_y and A_z) and ^{14}N superhyperfine (A^N_{iso}, A^N_x, A^N_y and A^N_z) coupling constants, and ^{14}N nuclear quadrupole coupling constant (NQCC or C_Q^N). The ^{51}V hyperfine coupling constants were calculated at the level of theory BHandHLYP/6-311g(d,p), with the functional BHandHLYP used as incorporated in the Gaussian 03 software. In the first-order approximation, the tensor $\boldsymbol{A}$ has one isotropic contribution derived from the Fermi contact (A_{iso}) and another from the dipolar hyperfine interaction (tensor $\boldsymbol{T}$): $\boldsymbol{A} = A_{iso}\mathbf{1} + \boldsymbol{T}$.[46,47,74] The values of the ^{51}V anisotropic hyperfine coupling constant along the x, y and z axes can be calculated by the equation: $A_x^{calcd.} = A_{iso} + T_x$; $A_y^{calcd.} = A_{iso} + T_y$; $A_z^{calcd.} = A_{iso} + T_z$, where A_{iso}, T_x, T_y and T_z can be read from the Gaussian 03 output. The A_z value (as well as A_x and A_y) is negative, but the literature usually report its absolute value and, therefore, the percent deviation from the experimental value is calculated as

$100 \times (|A_z|^{calcd.} - |A_z|^{exptl})/|A_z|^{exptl}$. The ^{14}N superhyperfine coupling constants were calculated at the level of theory BHandH/6-311+g(d,p); in this case the functional BHandH was also incorporated into the Gaussian 03 package.

The ^{14}N nuclear quadrupole coupling constant was evaluated from the electric field gradient (EFG) tensor, calculated with the functional B3PW91[75] and the basis set 6-311+g(d,p). C_Q^N is defined by $eQ^N V_z/h$, where e is the charge of an electron, Q^N the ^{14}N nuclear quadrupole moment (2.044 fm^2), V_z the largest component of the electric field gradient and h the Planck's constant. The asymmetry parameter is given by the expression $\eta = (V_x - V_y)/V_z$, with $|V_z| \geq |V_y| \geq |V_z|$.

Time-dependent density functional theory (TD-DFT) calculations,[61,76] used to predict the excited states of the $V^{IV}O^{2+}$ complexes and calculate the electronic absorption spectra, were based on the optimised geometry.

The analysis of molecular orbital (MO) composition in terms of atomic orbitals or groups of atoms was performed using the AOMix program.[77] The population analysis was calculated according to the procedure of Mulliken.[78] The generalised Wiberg (B_{AB}^W)[79] and Mayer (B_{AB}^M)[80] bond order indices for an A–B bond are given by Equations (5) and (6), respectively

$$B_{AB}^{W} = \sum_{a \in A} \sum_{b \in B} (\mathbf{PS})_{ab} (\mathbf{PS})_{ba} \quad (5)$$

$$B_{AB}^{M} = 2 \sum_{a \in A} \sum_{b \in B} \left[(\mathbf{P}^{\alpha}\mathbf{S})_{ab} (\mathbf{P}^{\alpha}\mathbf{S})_{ba} + (\mathbf{P}^{\beta}\mathbf{S})_{ab} (\mathbf{P}^{\beta}\mathbf{S})_{ba} \right] \quad (6)$$

where P, P^{α} and P^{β} are the total, and α- and β-spin density, respectively. In a general case with $P^{\alpha} \neq P^{\beta}$, the generalised Wiberg and Mayer bond orders are not equal.

Supporting Information (see also the footnote on the first page of this article): Table with calculated and experimental electronic transitions (Tables S1–S4), with composition of the highest occupied and lowest unoccupied molecular orbitals (Tables S5–S12) and Mayer bond indices (Table S13); figures with the optimised structures of $V^{IV}O^{2+}$ complexes (Figures S1–S6).

[1] a) D. C. Crans, J. J. Smee, E. Gaidamauskas, L. Yang, *Chem. Rev.* **2004**, *104*, 849–902; b) D. Rehder, *Bioinorganic Vanadium Chemistry*, Wiley, Chichester, **2008**.

[2] a) M. J. Smith, D. E. Ryan, K. Nakanishi, P. Frank, K. O. Hodgson, in: *Metal Ions in Biological Systems* (Eds.: A. Sigel, H. Sigel), Marcel Dekker, New York, **1995**, vol. 31, pp. 423–490; b) H. Michibata, T. Uyama, K. Kanamori, in: *Vanadium Compounds: Chemistry, Biochemistry and Therapeutic Applications* (Eds.: A. S. Tracey, D. C. Crans), ACS symposium series 711, Washington DC, **1998**, pp. 248–258.

[3] T. Ishii, I. Nakai, K. Okoshi, in: *Metal Ions in Biological Systems* (Eds.: A. Sigel, H. Sigel), Marcel Dekker, New York, **1995**, vol. 31, pp. 491–509.

[4] E. Bayer, in: *Metal Ions in Biological Systems* (Eds.: A. Sigel, H. Sigel), Marcel Dekker, New York, **1995**, vol. 31, pp. 407–421.

[5] a) H. Vilter, in: *Metal Ions in Biological Systems* (Eds.: A. Sigel, H. Sigel), Marcel Dekker, New York, **1995**, vol. 31, pp. 325–362; b) V. L. Pecoraro, C. A. Slebodnick, B. J. Hamstra, in: *Vanadium Compounds: Chemistry, Biochemistry and Therapeutic Applications* (Eds.: A. S. Tracey, D. C. Crans), ACS symposium series 711, Washington DC, **1998**, pp. 157–167.

[6] a) R. L. Robson, R. R. Eady, T. J. Richardson, R. W. Miller, M. Hawkins, J. R. Postgate, *Nature* **1986**, *322*, 388–390; b) R. R. Eady, in: *Metal Ions in Biological Systems* (Eds.: A. Sigel, H. Sigel), Marcel Dekker, New York, **1995**, vol. 31, pp. 363–405.

[7] F. H. Nielsen, in: *Metal Ions in Biological Systems* (Eds.: A. Sigel, H. Sigel), Marcel Dekker, New York, **1995**, vol. 31, pp. 543–573.

[8] P. J. Stankiewicz, A. S. Tracey, D. C. Crans, in: *Metal Ions in Biological Systems* (Eds.: A. Sigel, H. Sigel), Marcel Dekker, New York, **1995**, vol. 31, pp. 287–324.

[9] a) Y. Shechter, S. J. D. Karlish, *Nature* **1980**, *284*, 556–558; b) K. H. Thompson, J. H. McNeill, C. Orvig, *Chem. Rev.* **1999**, *99*, 2561–2571 and references cited therein; c) K. H. Thompson, C. Orvig, *Coord. Chem. Rev.* **2001**, *219–221*, 1033–1053 and references cited therein; d) Y. Shechter, I. Goldwaser, M. Mironchik, M. Fridkin, D. Gefel, *Coord. Chem. Rev.* **2003**, *237*, 3–11; e) K. Kawabe, Y. Yoshikawa, Y. Adachi, H. Sakurai, *Life Sci.* **2006**, *78*, 2860–2866.

[10] a) K. H. Thompson, C. Orvig, *J. Inorg. Biochem.* **2006**, *100*, 1925–1935; b) K. H. Thompson, J. Lichter, C. LeBel, M. C. Scaife, J. H. McNeill, C. Orvig, *J. Inorg. Biochem.* **2009**, *103*, 554–558.

[11] K. Kustin, W. E. Robinson, in: *Metal Ions in Biological Systems* (Eds.: A. Sigel, H. Sigel), Marcel Dekker, New York, **1995**, vol. 31, pp. 511–542.

[12] T. Kiss, T. Jakusch, D. Hollender, A. Dörnyei, E. A. Enyedy, J. Costa Pessoa, H. Sakurai, A. Sanz-Medel, *Coord. Chem. Rev.* **2008**, *252*, 1153–1162 and references cited therein.

[13] a) K. Kustin, D. L. Toppen, *Inorg. Chem.* **1973**, *12*, 1404–1407; b) L. C. Cantley Jr., J. H. Ferguson, K. Kustin, *J. Am. Chem. Soc.* **1978**, *100*, 5210–5212; c) H. Sakurai, S. Shimomura, K. Ishizu, *Inorg. Chim. Acta* **1978**, *55*, L67–L69; d) P. C. Wilkins, M. D. Johnson, A. A. Holder, D. C. Crans, *Inorg. Chem.* **2006**, *45*, 1471–1479.

[14] N. D. Chasteen, in: *Metal Ions in Biological Systems* (Eds.: A. Sigel, H. Sigel), Marcel Dekker, New York, **1995**, vol. 31, pp. 231–247.

[15] C. Harford, B. Sarkar, *Acc. Chem. Res.* **1997**, *30*, 123–130.

[16] T. Kiss, T. Jakusch, J. Costa Pessoa, I. Tomaz, *Coord. Chem. Rev.* **2003**, *237*, 123–133 and references cited therein.

[17] C. R. Cornman, E. P. Zovinka, Y. D. Boyajina, K. M. Geisre-Bush, P. D. Boyle, P. Singh, *Inorg. Chem.* **1995**, *34*, 4213–4219.

[18] A. D. Keramidas, A. P. Papaioannou, A. Vlahos, T. A. Kabanos, G. Bonas, A. Makriyannis, C. P. Raptopoulou, A. Terzis, *Inorg. Chem.* **1996**, *35*, 357–367.

[19] A. J. Tasopoulos, A. T. Vlahos, A. D. Keramidas, T. A. Kabanos, Y. G. Deligiannakis, C. P. Raptopoulou, A. Terzis, *Angew. Chem. Int. Ed. Engl.* **1996**, *35*, 2531–2533.

[20] A. J. Tasiopoulos, A. N. Troganis, A. Evangelou, C. P. Raptopoulou, A. Terzis, Y. Deligiannakis, T. A. Kabanos, *Chem. Eur. J.* **1999**, *5*, 910–921.

[21] A. T. Vlahos, E. I. Tolis, C. P. Raptopoulou, A. Tsohos, M. P. Sigalas, A. Terzis, T. A. Kabanos, *Inorg. Chem.* **2000**, *39*, 2977–2985.

[22] E. J. Tolis, V. I. Teberekidis, C. P. Raptopoulou, A. Terzis, M. Sigalas, Y. Deligiannakis, T. A. Kabanos, *Chem. Eur. J.* **2001**, *7*, 2698–2710.

[23] A. J. Tasiopoulos, E. J. Tolis, J. M. Tsangaris, A. Evangelou, J. D. Woollins, A. M. Z. Slawin, J. Costa Pessoa, I. Correia, T. A. Kabanos, *J. Biol. Inorg. Chem.* **2002**, *7*, 363–374.

[24] T. Jakusch, A. Dörnyei, I. Correia, L. M. Rodriguez, G. K. Tóth, T. Kiss, J. Costa Pessoa, S. Marcão, *Eur. J. Inorg. Chem.* **2003**, 2113–2122.

[25] E. Garribba, E. Lodyga-Chruscinska, G. Micera, A. Panzanelli, D. Sanna, *Eur. J. Inorg. Chem.* **2005**, 1369–1382 and references cited therein.

[26] E. Garribba, G. Micera, E. Lodyga-Chruscinska, D. Sanna, G. Sanna, *Eur. J. Inorg. Chem.* **2005**, 4953–4963.

[27] K. Várnagy, T. Csorba, D. Kiss, E. Garribba, G. Micera, D. Sanna, *Eur. J. Inorg. Chem.* **2007**, 4884–4896.

[28] L. Pisano, D. Kiss, K. Várnagy, D. Sanna, G. Micera, E. Garribba, *Eur. J. Inorg. Chem.* **2009**, 2362–2374.

[29] F. Neese, *Coord. Chem. Rev.* **2009**, *253*, 526–563 and references cited therein.

[30] M. J. Frisch, G. W. Trucks, H. B. Schlegel, G. E. Scuseria, M. A. Robb, J. R. Cheeseman, J. A. Montgomery Jr., T. Vreven, K. N. Kudin, J. C. Burant, J. M. Millam, S. S. Iyengar, J. Tomasi, V. Barone, B. Mennucci, M. Cossi, G. Scalmani, N. Rega, G. A. Petersson, H. Nakatsuji, M. Hada, M. Ehara, K. Toyota, R. Fukuda, J. Hasegawa, M. Ishida, T. Nakajima, Y. Honda, O. Kitao, H. Nakai, M. Klene, X. Li, J. E. Knox, H. P. Hratchian, J. B. Cross, C. Adamo, J. Jaramillo, R. Gomperts, R. E. Stratmann, O. Yazyev, A. J. Austin, R. Cammi, C. Pomelli, J. W. Ochterski, P. Y. Ayala, K. Morokuma, G. A. Voth, P. Salvador, J. J. Dannenberg, V. G. Zakrzewski, S. Dapprich, A. D. Daniels, M. C. Strain, O. Farkas, D. K. Malick, A. D. Rabuck, K. Raghavachari, J. B. Foresman, J. V. Ortiz, Q. Cui, A. G. Baboul, S. Clifford, J. Cioslowski, B. B. Stefanov, G. Liu, A. Liashenko, P. Piskorz, I. Komaromi, R. L. Martin, D. J. Fox, T. Keith, M. A. Al-Laham, C. Y. Peng, A. Nanayakkara, M. Challacombe, P. M. W. Gill, B. Johnson, W. Chen, M. W. Wong, C. Gonzalez, J. A. Pople, *Gaussian 03*, Revision C.02, Gaussian, Inc., Wallingford CT, **2004**.

[31] a) M. Bühl, H. Kabrede, *J. Chem. Theory Comput.* **2006**, *2*, 1282–1290; b) M. P. Waller, M. Bühl, *J. Comput. Chem.* **2007**, *28*, 1531–1537; c) M. P. Waller, H. Braun, N. Hojdis, M. Bühl, *J. Chem. Theory Comput.* **2007**, *3*, 2234–2242; d) M. Bühl, C. Reimann, D. A. Pantazis, T. Bredow, F. Neese, *J. Chem. Theory Comput.* **2008**, *4*, 1449–1459.

[32] P. Comba, M. Kerscher, *Coord. Chem. Rev.* **2009**, *253*, 564–574.

[33] A. D. Becke, *J. Chem. Phys.* **1993**, *98*, 5648–5652.

[34] C. Lee, W. Yang, R. G. Parr, *Phys. Rev. B* **1998**, *37*, 785–789.

[35] a) K. G. Spears, *J. Phys. Chem. A* **1997**, *101*, 6273–6279; b) C. P. Aznar, Y. Deligiannakis, E. J. Tolis, T. Kabanos, M. Brynda, R. D. Britt, *J. Phys. Chem. A* **2004**, *108*, 4310–4321; c) I. Correia, J. Costa Pessoa, M. T. Duarte, R. T. Henriques, M. F. M. Piedade, L. F. Veiros, T. Jakusch, T. Kiss, Á. Dörnyei, M. M. C. A. Castro, C. F. G. C. Geraldes, F. Avecilla, *Chem. Eur. J.* **2004**, *10*, 2301–2317; d) L. L. G. Justino, M. L. Ramos, F. Nogueira, A. J. F. N. Sobral, C. F. G. C. Geraldes, M. Kaupp, H. D. Burrows, C. Fiolhais, V. M. S. Gil, *Inorg. Chem.* **2008**, *47*, 7317–7326.

[36] E. Garribba, G. Micera, D. Sanna, in: *6th Int. Symp. Vanadium Chem*. Lisbon, **2008**, book of abstracts, O30.

[37] H. Sakurai, Z. Taira, N. Sakai, *Inorg. Chim. Acta* **1988**, *151*, 85–86.

[38] N. D. Chasteen, in: *Biological Magnetic Resonance* (Eds.: L. J. Berliner, J. Reuben), Plenum Press, New York, **1981**, vol. 3, pp. 53–119.

[39] C. D. Garner, D. Collison, F. E. Mabbs, in: *Metal Ions in Biological Systems* (Eds.: A. Sigel, H. Sigel), Marcel Dekker, New York, **1995**, vol. 31, pp. 617–670.

[40] G. Micera, D. Sanna, in: *Vanadium in the Environment Part 1: Chemistry and Biochemistry* (Ed.: J. O. Nriagu), Wiley, New York, **1998**, pp. 131–166.

[41] T. S. Smith II, R. LoBrutto, V. L. Pecoraro, *Coord. Chem. Rev.* **2002**, *228*, 1–18.

[42] S. A. Dikanov, Y. D. Tsvetkov, *Electron Spin Echo Envelope Modulation (ESEEM) Spectroscopy*, CRC Press, Boca Raton, **1992**.

[43] A. Schweiger, *Angew. Chem. Int. Ed. Engl.* **1991**, *30*, 265–292.

[44] Y. Deligiannakis, M. Louloudi, N. Hadjiliadis, *Coord. Chem. Rev.* **2000**, *204*, 1–112.

[45] a) *Calculation of NMR and EPR Parameters. Theory and Applications* (Eds.: M. Kaupp, M. Bühl, V. G. Malkin), Wiley-VCH, Weinheim, **2004**; b) C. Remenyi, R. Reviakine, A. V. Arbuznikov, J. Vaara, M. Kaupp, *J. Phys. Chem. A* **2004**, *108*, 5026–5033, and references cited therein.

[46] a) M. L. Munzarová, M. Kaupp, *J. Phys. Chem. B* **2001**, *105*, 12644–12652, and references cited therein.

[47] a) A. C. Saladino, S. C. Larsen, *J. Phys. Chem. A* **2003**, *107*, 1872–1878; b) A. C. Saladino, S. C. Larsen, *Catal. Today* **2005**, *105*, 122–133 and references cited therein.

[48] F. Neese, *J. Chem. Phys.* **2003**, *118*, 3939–3948.

[49] G. Micera, E. Garribba, *Dalton Trans.* **2009**, 1914–1918.

[50] R. G. Hayes, *Inorg. Chem.* **2000**, *39*, 156–158.

[51] F. Neese, *J. Phys. Chem. A* **2001**, *105*, 4290–4299.

[52] A. C. Saladino, S. C. Larsen, *J. Phys. Chem. A* **2003**, *107*, 4735–4740.

[53] W. M. Ames, S. C. Larsen, *Phys. Chem. Chem. Phys.* **2009**, *11*, 8266–8274.

[54] K. Fukui, H. Fujii, H. Ohya-Nishiguchi, H. Kamada, *Chem. Lett.* **2000**, 198–199.

[55] E. J. Reijerse, J. Shane, E. de Boer, P. Höfer, D. Collison, in: *Electron Magnetic Resonance of Disordered Systems* (Ed.: N. D. Yordanov), World Scientific, Singapore, **1991**, vol. 31, pp. 253–271.

[56] A convenient quantum mechanical concept to be used in these cases is the spin population ρ_N^{Ψ}, where N is the nucleus of the atom in question, and Ψ stands for the orbital. The spin population may be interpreted as an integrated spin density $\rho_S(x,y,z)$ in the orbital Ψ centred on the nucleus N and is the difference in the populations of unpaired electrons with spin up or α (positive spin) and spin down or β (negative spin): $\rho_N^{\Psi} = \rho_N^{\psi,\alpha} - \rho_N^{\psi,\beta}$. As for $\rho_S(x,y,z)$, the spin population ρ_N^{Ψ} can be positive, zero or negative: a positive value (positive spin population) signifies that the probability of finding the unpaired electron with the conventional spin α in the orbital ψ is larger than that for the spin β, and a negative value (negative spin population) indicates the opposite situation. In contrast to the spin density $\rho_S(x,y,z)$, which is in units of m^{-3}, the spin population ρ_N^{Ψ} is dimensionless.

[57] a) K. Fukui, H. Ohya-Nishiguchi, H. Kamada, *Inorg. Chem.* **1997**, *36*, 5518–5529; b) K. Fukui, T. Ueki, H. Ohya, H. Michibata, *J. Am. Chem. Soc.* **2003**, *125*, 6352–6353.

[58] a) S. C. Larsen, D. J. Singel, *J. Phys. Chem.* **1992**, *96*, 9007–9013; b) R. S. Magliozzo, J. Peisach, *Biochemistry* **1993**, *32*, 8446–8456; c) K. Fukui, H. Ohya-Nishiguchi, H. Kamada, *J. Phys. Chem.* **1993**, *97*, 11858–11860; d) E. J. Reijerse, A. M. Tyryshkin, S. A. Dikanov, *Magn. Reson.* **1998**, *131*, 295–309.

[59] K. J. Ooms, S. E. Bolte, B. Baruah, M. Aziz Choudhary, D. C. Crans, T. Polenova, *Dalton Trans.* **2009**, 3262–3269.

[60] I. Sóvágó, in: *Biocoordination Chemistry* (Ed.: K. Burger), Ellis Horwood, New York, **1990**, pp. 135–184.

[61] M. E. Casida, in: *Recent Advances in Density Functional Methods* (Ed.: D. P. Chong), World Scientific, Singapore, **1995**, vol. 1, pp. 155–192.

[62] A. Rosa, G. Ricciardi, O. Gritsenko, E. J. Berends, *Struct. Bonding (Berlin)* **2004**, *112*, 49–115.

[63] The oscillator strength of an electric dipole transition is $f = [2m_e(E_\kappa - E_l)/3e^2\hbar^2] \times |\mu_{\kappa l}|^2$, where $(E_\kappa - E_l)$ and $\mu_{\kappa l}$ are the energy and transition dipole moment for a transition from an initial state l to a final state k. The oscillator strength can be related to the absorbance A of a band (and hence to its molar absorption coefficient) through the equation $f = (4m_e c\varepsilon_0/N_A e^2) \times A$.

[64] C. J. Ballhausen, H. B. Gray, *Inorg. Chem.* **1962**, *1*, 111–122.

[65] a) Y.-L. Chen, S.-W. Lee, Y. Chi, K.-C. Hwang, S. B. Kumar, Y.-H. Hu, Y.-M. Cheng, P.-T. Chou, S.-M. Peng, G.-H. Lee, S.-J. Yeh, C.-T. Chen, *Inorg. Chem.* **2005**, *44*, 4287–4294; b) S. I. Gorelsky, L. Basumallick, J. Vura-Weis, R. Sarangi, K. O. Hodgson, B. Hedman, K. Fujisawa, E. I. Solomon, *Inorg. Chem.* **2005**, *44*, 4947–4960; c) A. T. Chaviara, A. C. Tsipis, P. J. Cox, C. A. Bolos, *Eur. J. Inorg. Chem.* **2005**, 3491–3502; d) M.-F. Charlot, Y. Pellegrin, A. Quaranta, W. Leibl, A. Aukauloo,

Chem. Eur. J. **2006**, *12*, 796–812; e) D. A. Jose, P. Kar, D. Koley, B. Ganguly, W. Thiel, H. N. Ghosh, A. Das, *Inorg. Chem.* **2007**, *46*, 5576–5584; f) B. Machura, R. Kruszynski, J. Kusz, *Polyhedron* **2007**, *26*, 1590–1596; g) M. Orio, C. Philouze, O. Jarjayes, F. Neese, F. Thomas, *Inorg. Chem.* **2010**, *49*, 646–658.

[66] K. Wüthrich, *Helv. Chim. Acta* **1965**, *48*, 1012–1017.

[67] B. J. Hamstra, A. P. L. Houseman, G. J. Colpas, J. W. Kampf, R. LoBrutto, W. D. Frasch, V. L. Pecoraro, *Inorg. Chem.* **1997**, *36*, 4866–4874.

[68] T. S. Smith II, C. A. Roof, J. W. Kampf, P. G. Rasmussen, V. L. Pecoraro, *J. Am. Chem. Soc.* **2000**, *122*, 767–775.

[69] T. Jakusch, P. Buglyó, A. I. Tomaz, J. Costa Pessoa, T. Kiss, *Inorg. Chim. Acta* **2002**, *339*, 119–128.

[70] M. M. Cosper, F. Neese, A. V. Astashkin, M. D. Carducci, A. M. Raitsimring, J. H. Enemark, *Inorg. Chem.* **2005**, *44*, 1290–1301.

[71] R. Kapre, K. Ray, I. Silvestre, T. Weyhermüller, S. DeBeer George, F. Neese, K. Wieghardt, *Inorg. Chem.* **2006**, *45*, 3499–3509.

[72] A. V. Astashkin, F. Neese, A. M. Raitsimring, J. J. A. Cooney, E. Bultman, J. H. Enemark, *J. Am. Chem. Soc.* **2005**, *127*, 16713–16722.

[73] R. G. Parr, W. Yang, *Density-Functional Theory of Atoms and Molecules*, Oxford University Press, Oxford, **1989**.

[74] a) R. S. Drago, *Physical Methods in Chemistry*, Saunders, Philadelphia, **1977**; b) J. E. Wertz, J. R. Bolton, *Electron Spin Resonance: Elementary Theory and Practical Applications*, Chapman and Hall, New York, **1986**.

[75] a) J. P. Perdew, in: *Electronic Structure of Solids* (Eds.: P. Ziesche, H. Eischrig), Akademie Verlag, Berlin, **1991**, pp. 11–20; b) J. P. Perdew, Y. Wang, *Phys. Rev. B* **1992**, *45*, 13244–13249.

[76] E. Runge, E. K. U. Gross, *Phys. Rev. Lett.* **1984**, *52*, 997–1000.

[77] a) S. I. Gorelsky, *AOMix program*, http://www.sg-chem.net, University of Ottawa, **2009**; b) S. I. Gorelsky, A. B. P. Lever, *J. Organomet. Chem.* **2001**, *635*, 187–196.

[78] a) R. S. Mulliken, *J. Chem. Phys.* **1955**, *23*, 1833–1840; b) R. S. Mulliken, *J. Chem. Phys.* **1955**, *23*, 1841–1846; c) R. S. Mulliken, *J. Chem. Phys.* **1955**, *23*, 2338–2342; d) R. S. Mulliken, *J. Chem. Phys.* **1955**, *23*, 2343–2346.

[79] K. B. Wiberg, *Tetrahedron* **1968**, *24*, 1083–1096.

[80] a) I. Mayer, *Chem. Phys. Lett.* **1984**, *110*, 440–444; b) I. Mayer, *Theor. Chim. Acta* **1985**, *67*, 315–322; c) I. Mayer, *Int. J. Quantum Chem.* **1986**, *29*, 73–84; d) I. Mayer, *Int. J. Quantum Chem.* **1986**, *29*, 477–483.

Received: April 6, 2010
Published Online: August 24, 2010
Please note: Minor changes have been made to this manuscript since its publication in *European Journal of Inorganic Chemistry* Early View. The Editor.

